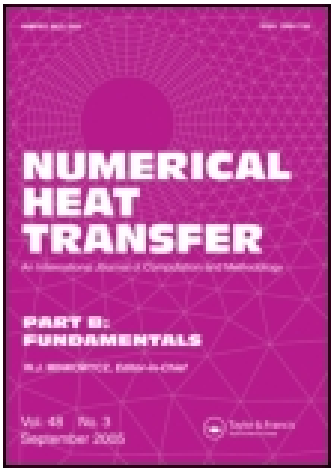

Numerical Heat Transfer, Part B: Fundamentals: An International Journal of Computation and Methodology
Publication details, including instructions for authors and subscription information:
http://www.tandfonline.com/loi/unhb20

DEVELOPMENT OF A GENERALIZED ZONAL METHOD FOR ANALYSIS OF RADIATIVE TRANSFER IN ABSORBING AND ANISOTROPICALLY SCATTERING MEDIA

W. W. Yuen [a] & E. E. Takara [a]
[a] Department of Mechanical and Environmental Engineering , University of California , Santa Barbara, California, USA
Published online: 13 Jul 2010.

To cite this article: W. W. Yuen & E. E. Takara (1994) DEVELOPMENT OF A GENERALIZED ZONAL METHOD FOR ANALYSIS OF RADIATIVE TRANSFER IN ABSORBING AND ANISOTROPICALLY SCATTERING MEDIA, Numerical Heat Transfer, Part B: Fundamentals: An International Journal of Computation and Methodology, 25:1, 75-96, DOI: 10.1080/10407799408955911

To link to this article: http://dx.doi.org/10.1080/10407799408955911

DEVELOPMENT OF A GENERALIZED ZONAL METHOD FOR ANALYSIS OF RADIATIVE TRANSFER IN ABSORBING AND ANISOTROPICALLY SCATTERING MEDIA

W. W. Yuen and E. E. Takara
Department of Mechanical and Environmental Engineering, University of California, Santa Barbara, California, USA

The generalized zonal method (GZM) for the analysis of radiative heat transfer in absorbing, emitting, and anisotropically scattering media is developed and implemented. It is shown to be applicable both for media with arbitrary scattering phase function and general nondiffuse reflecting surfaces. Mathematically, the GZM is a generalization of the conventional zonal method (CZM). In addition to the exchange factors utilized by the CZM, the GZM introduces scattering and reflecting exchange factors. These factors characterize the scattering properties of the medium and the reflectivities of the bounding surfaces. Expressions for the scattering and reflecting exchange factors are shown; their numerical and analytical properties are identified. To illustrate the implementation of the GZM, cubic enclosures in radiative equilibrium are analyzed. Based on numerical data, the effect of anisotropic scattering on three-dimensional radiative heat transfer is assessed.

The importance of radiation heat transfer in many practical engineering systems is well known. In furnaces, boilers, and other high-temperature systems, radiation is known to be the dominant heat transfer mechanism [1–3]. In superinsulation systems, both conductive and convective heat transfer can be effectively curtailed [4–6]. To optimize the performance of these systems, proper analysis of radiation heat transfer is critical.

Due to the mathematical complexity of radiative heat transfer, a great deal of effort has been directed toward the development of many approximation methods. The applicability of these methods depends on the nature of the physical system, the characteristics of the medium, the degree of accuracy required, and the availability of computer facilities. Currently used methods include the multiflux methods [7–11], moment methods [12, 13], spherical harmonics (P_n approximation) [14, 15], and the discrete-ordinate approximation [16, 17]. To verify the accuracy of

Received 24 May 1993; accepted 11 September 1993.

This article is based on work supported by the National Science Foundation under grant no. CTS-8915042. Some of the computational work was done at the UCSD and UCLA supercomputer centers under block time grants.

Address correspondence to W. W. Yuen, Department of Mechanical and Environmental Engineering, University of California, Santa Barbara, CA 93106.

Numerical Heat Transfer, Part B, 25:75–96, 1994

1040–7790/94 $10.00 + .00

NOMENCLATURE

A_i	area element i	S_{gi}	net radiant absorption by volume element i
B	percentage change in the bottom wall heat flux due to scattering in the example calculation	T	percentage change in the top wall heat flux due to scattering in the example calculation
E_{gi}	emissive power from volume element i	W_{gi}	radiosity from volume element i
E_i	emissive power from area element i	$W_{gi,j}$	directional radiosity from volume element i to area element J
g_ig_j	exchange factor between volumes V_i and V_j, Eq. (1)	$W_{gi,gj}$	directional radiosity from volume element i to volume element J
g_is_j	exchange factor between volume V_i and area A_j, Eq. (2)	W_i	radiosity from area element i
H_{gi}	average irradiation into volume element i	$W_{i,j}$	directional radiosity from area element i to area element J
H_i	average irradiation into area element i	$W_{i,gj}$	directional radiosity from area element i to volume element J
K_t	extinction coefficient	$\mathbf{W}_i$	radiosity vector whose components are $W_{i,j}$
L	dimension used in example calculation	$\tilde{\mathbf{W}}$	generalized radiosity vector whose components are $\mathbf{W}_i$
$\mathbf{n}_i$	nit normal vector at area element i	β	forward-backward scattering parameter used in Eq. (40)
q_b	heat flux at the bottom wall in the example calculation	ϵ_i	emissivity of area element i
q_i	heat flux at area element i	θ	scattering angle used in Eq. (40)
q_s	heat flux at the side wall in the example calculation	$\hat{\rho}_{k,i,j}$	average reflectivities defined by Eq. (19)
q_t	heat flux at the top wall in the example calculation	$\hat{\rho}_{gk,i,j}$	average reflectivities defined by Eq. (20)
Q_i	heat transfer from area element i	$\hat{\rho}_{gk,i,gj}$	average reflectivities defined by Eq. (21)
r_{ij}	distance between area (or volume) element i and area (or volume) element j defined by Eq. (5)	$\hat{\Phi}$	scattering phase function defined by Eq. (24)
$\mathbf{r}_{ij}$	vector pointing from area (or volume) element i and area (or volume) element j defined by Eq. (4)	$\hat{\Phi}_{i,gj,k}$	average phase function defined by Eq. (24)
s_is_j	exchange factor between areas A_i and A_j, Eq. (3)	$\hat{\Phi}_{gi,gj,k}$	average function defined by Eq. (25)
S	percentage change in the side wall heat flux due to scattering in the example calculation	$\hat{\Phi}_{gi,gj,gk}$	average phase function defined by Eq. (26)
		ω_0	scattering albedo

these methods, benchmark numerical solutions generated by the CZM [18] and/or the Monte Carlo method (MCM) [19, 20] are used.

However, both the CZM and MCM have limitations in generating benchmark solutions. The CZM is not applicable for problems with anisotropically scattering media and general nondiffuse surfaces. The MCM becomes computationally prohibitive when the scattering albedo and surface reflectivity become high. The lack of benchmark numerical solutions generated by established numerical procedures has led to uncertainty in the accuracy of all approximation methods for this class of problems. For example, most of the existing numerical predictions for practical

furnaces (which generally contain highly anisotropically scattering combustion products) have unknown accuracy. While some of these calculations were successful in correlating experimental data [21], it is doubtful that they can be used reliably as a basis for engineering design.

The need for benchmark solutions has been addressed to a certain extent by the symposium on radiative heat transfer in the 1992 Heat Transfer Conference [22]. The various methods presented there included the GZM [23], discretized radiosity [24], YIX [25], a modified Monte Carlo method [26], and K distribution [27]. Due to the nature of the symposium, detailed descriptions of the methods were not given. While no method was clearly superior, the GZM showed promise.

In this article, a detailed development and implementation of the GZM is presented. Mathematically, the GZM is demonstrated to be a vector generalization of the CZM, based on a radiosity-irradiation approach [28, 29]. Next, the basic conservation equations for the GZM are derived. The scattering and reflecting exchange factors are introduced. They characterize the scattering property of the medium and the reflecting property of the enclosed surface, respectively. The analytical and numerical properties of these exchange factors are presented. Lastly, cubic enclosures in radiative equilibrium are analyzed. Based on these results, the effect of anisotropic scattering on multidimensional radiative heat transfer is illustrated.

MATHEMATICAL FORMULATION

The Conventional Zonal Method (CZM)

Since the GZM is a generalization of the CZM, the basic concepts and equations of the CZM are outlined here. The assumptions and details were presented by Hottel and Sarofim [18] and will not be repeated. For an enclosure with M volume zones and N surface zones, CZM utilizes three basic exchange factors:

$$g_i g_j = \int_{V_i}\int_{V_j} \frac{K_t^2 e^{-K_t r_{ij}}\, dV_i\, dV_j}{\pi r_{ij}^2} \tag{1}$$

$$g_i s_j = \int_{A_i}\int_{V_j} \frac{K_t(\mathbf{r}_{ij}\cdot\mathbf{n}_j) e^{-K_t r_{ij}}\, dV_i\, dA_j}{\pi r_{ij}^3} \tag{2}$$

$$s_i s_j = \int_{A_i}\int_{A_j} \frac{(\mathbf{r}_{ij}\cdot\mathbf{n}_i)(\mathbf{r}_{ij}\cdot\mathbf{n}_j) e^{-K_t r_{ij}}\, dA_i\, dA_j}{\pi r_{ij}^4} \tag{3}$$

with

$$\mathbf{r}_{ij} = (x_j - x_i)\mathbf{i} + (y_j - y_i)\mathbf{j} + (z_j - z_i)\mathbf{k} \tag{4}$$

$$r_{ij} = \left[(x_i - x_j)^2 + (y_i - y_j)^2 + (z_i - z_j)^2\right]^{1/2} \tag{5}$$

and

K_t = extinction coefficient (assumed constant)

$\mathbf{n}_i$ = unit normal at surface dA_i

$\mathbf{n}_j$ = unit normal at surface dA_j

$g_i g_j$ is the exchange factor between volume zones V_i and V_j, $g_i s_j$ is the exchange factor between volume zone V_i and area zone A_j, and $s_i s_j$ is the exchange factor between area zones A_i and A_j.

Radiative equilibrium in an enclosure is expressed in terms of the radiosity and irradiation for each volume zone V_i and area zone A_i. Letting

W_i = radiosity from A_i (emission plus reflection)

E_i = emissive power from A_i

H_i = "averrage" irradiation into A_i

Q_i = net heat transfer from A_i

ϵ_1 = emissivity of surface A_i

and

$\frac{K_t W_{gi}}{\pi}$ = outgoing radiosity from V_i (emission plus reflection)

E_{gi} = emissive power from V_i

$\frac{H_{gi}}{\pi}$ = "average" incoming intensity into V_i

S_{gi} = net radiant absorption by volume zone V_i

ω_0 = scattering albedo of volume zone V_i

the energy balance at A_i and V_i can be written as

$$W_i = \epsilon_i E_i + (1 - \epsilon_i) H_i \qquad i = 1, N \tag{6}$$

$$Q_i = A_i(W_i - H_i) = \frac{A_i \epsilon_i}{1 - \epsilon_i}(E_i - W_i) \qquad i = 1, N \tag{7}$$

and

$$W_{gi} = (1 - \omega_0) E_{gi} + \omega_0 H_{gi} \qquad i = 1, M \tag{8}$$

$$S_{gi} = 4K_t V_i(H_{gi} - W_{gi}) = 4K_t V_i \left(\frac{1 - \omega_0}{\omega_0} \right)(W_{gi} - E_{gi}) \qquad i = 1, M \tag{9}$$

The overall energy balance at V_i and A_i in terms of its exchange with the remaining zones can be written as

$$A_i H_i = \sum_{j=1}^{N} (s_i s_j) W_j + \sum_{j=1}^{M} (s_i g_j) W_{gj} \qquad i = 1, N \tag{10}$$

$$4K_t V_i H_{gi} = \sum_{j=1}^{N} (g_i s_j) W_j + \sum_{j=1}^{M} (g_i g_j) W_{gj} \qquad i = 1, M \tag{11}$$

Equations (1)–(11) constitute the complete set of mathematical relations required by CZM. In general, either Q_i (S_{gi}) or E_i (E_{gi}) is specified on each surface zone (or volume zone). Equations (6)–(10) can be readily combined to yield the following matrix equation for the unknown enclosure radiosity vector $\mathbf{W}$ ($W_1, W_2, \ldots, W_N, W_g1, W_g2, \ldots, W_gM$):

$$\mathbf{W} = \tilde{\mathbf{X}}\mathbf{J} + \tilde{\mathbf{Y}}\mathbf{W} \tag{12}$$

where $\tilde{\mathbf{X}}$ is an NM by NM diagonal matrix whose components are functions of ϵ_i, ω_0, A_i, and V_i, and $\tilde{\mathbf{Y}}$ is an NM by NM full matrix whose components are the various exchange factors. $\mathbf{J}$ is a source vector composed of the specified emissive powers or heat fluxes. The solution to Eq. (12) can be readily obtained. The success of the CZM for enclosures with an isotropically scattering medium and diffusely reflecting surface is well documented [3].

The Generalized Zonal Method (GZM)

The most severe limitation of the CZM is the assumption that the volume radiosity, W_{gi}, and surface radiosity, W_i, are isotropic. This restricts the CZM to diffuse/isotropic enclosures. In the GZM, this assumption is eliminated. The directional dependence of radiosity (due to anisotropic scattering and nondiffuse reflection) is included in the formulation. The radiosity of each zone is generalized to become an vector with NM components. For example, $W_{i,j}$ and $W_{i,gj}$ are the average radiosities from area A_i to area A_j and volume V_j. Likewise, $W_{gi,j}$ and $W_{gi,gj}$ are the average radiosities from volume V_i to area A_j and volume zone V_j.

The radiosity components are assumed to be constant in the exchange calculation for each pair of zonal elements. As the number of zones increase the directional dependencies of radiosity will be better simulated and the accuracy of numerical results can be expected to improve. Mathematically, equations (10) and (11) for CZM are now replaced by

$$A_i H_i = \sum_{j=1}^{N} (s_i s_j) W_{j,i} + \sum_{j=1}^{M} (s_i g_j) W_{gj,i} \qquad i = 1, N \tag{13}$$

$$4K_t V_i H_{gi} = \sum_{j=1}^{N} (g_i s_j) W_{j,gi} + \sum_{j=1}^{M} (g_i g_j) W_{gj,gi} \qquad i = 1, M \tag{14}$$

Equations (7) and (9) become

$$Q_i = \sum_{j=1}^{N} (s_i s_j)(W_{i,j} - W_{j,i}) + \sum_{j=1}^{M} (s_i g_j)(W_{i,gj} - W_{gj,i}) \qquad i = 1, N \quad (15)$$

and

$$S_{gi} = \sum_{j=1}^{N} (g_i s_j)(W_{gi,j} - W_{j,gi}) + \sum_{j=1}^{M} (g_i g_j)(W_{gi,gj} - W_{gj,gi}) \qquad i = 1, M \quad (16)$$

The radiosity vectors $\mathbf{W}_i$ and $\mathbf{W}_{gi}$ are related by the scattering properties of the medium and the reflective properties of the surfaces. The components of $\mathbf{W}_i$, the radiosity vector of surface zone A_i, are written as

$$W_{i,j} = \epsilon_i E_i + \frac{\pi}{A_i} \sum_{k=1}^{N} W_{k,i} \hat{\rho}_{k,i,j}(s_i s_k) + \frac{\pi}{A_i} \sum_{l=1}^{M} W_{gl,i} \hat{\rho}_{gl,i,j}(s_i g_l) \qquad j = 1, N \quad (17)$$

and

$$W_{i,gj} = \epsilon_i E_i + \frac{\pi}{A_i} \sum_{k=1}^{N} W_{k,i} \hat{\rho}_{k,i,gj}(s_i s_k) + \frac{\pi}{A_i} \sum_{l=1}^{M} W_{gl,i} \hat{\rho}_{gl,i,gj}(s_i g_l) \qquad j = 1, M \quad (18)$$

$\hat{\rho}_{k,i,j}$, $\hat{\rho}_{gl,i,j}$, and $\hat{\rho}_{gl,i,gj}$ are averaged reflectivities at surface A_i given by

$$\hat{\rho}_{k,i,j} = \frac{A_i}{(s_i s_k)(s_i s_j)} \int_{A_j} \int_{A_i} \int_{A_k} \rho''(\mathbf{r}_i, \theta_{ji}, \phi_{ji}, \theta_{ki}, \phi_{ki}) e^{-K_t(r_{ji}+r_{ki})} \times \frac{(\mathbf{r}_{ji} \cdot \mathbf{n}_i)(\mathbf{r}_{ji} \cdot \mathbf{n}_j)(\mathbf{r}_{ki} \cdot \mathbf{n}_i)(\mathbf{r}_{ki} \cdot \mathbf{n}_k)}{\pi^2 r_{ji}^4 r_{ki}^4} dA_k \, dA_i \, dA_j \quad (19)$$

$$\hat{\rho}_{gl,i,j} = \frac{A_i}{(s_i g_l)(s_i s_j)} \int_{V_l} \int_{A_i} \int_{A_j} \rho''(\mathbf{r}_i, \theta_{ji}, \phi_{ji}, \theta_{li}, \phi_{li}) e^{-K_t(r_{ji}+r_{li})} \times \frac{(\mathbf{r}_{ji} \cdot \mathbf{n}_i)(\mathbf{r}_{ji} \cdot \mathbf{n}_j)(\mathbf{r}_{li} \cdot \mathbf{n}_i)}{\pi^2 r_{ji}^3 r_{li}^4} K_t \, dA_j \, dA_i \, dV_l \quad (20)$$

$$\hat{\rho}_{gl,i,gj} = \frac{A_i}{(s_i g_l)(s_i g_l)} \int_{V_l} \int_{A_i} \int_{V_j} \rho''(\mathbf{r}_i, \theta_{li}, \phi_{li}, \theta_{ji}, \phi_{ji}) e^{-K_t(r_{ji}+r_{li})} \times \frac{(\mathbf{r}_{ji} \cdot \mathbf{n}_i)(\mathbf{r}_{li} \cdot \mathbf{n}_i)}{\pi^2 r_{ji}^3 r_{li}^3} K_t^2 \, dV_l \, dA_i \, dV_j \quad (21)$$

$\rho''(\mathbf{r}_i, \theta_{ji}, \phi_{ji}, \theta_{ki}, \phi_{ki})$ is the bidirectional reflectivity of A_i at $\mathbf{r}_i$ for radiation incident in the (θ_{ji}, ϕ_{ji}) direction and reflecting in the (θ_{ik}, ϕ_{ik}) direction.

Likewise, the components of $\mathbf{W}_{gi}$, the radiosity vector of volume zone V_i, are

$$W_{gi,j} = (1 - \omega_0)E_{gi} + \frac{\omega_0}{4K_tV_i}\sum_{k=1}^{N} W_{k,gi}\hat{\Phi}_{k,gi,j}(g_is_k) + \frac{\omega_0}{4K_tV_i}\sum_{l=1}^{M} W_{gl,gi}\hat{\Phi}_{gl,gi,j}(g_ig_l) \qquad j = 1, N \tag{22}$$

and

$$W_{gi,gj} = (1 - \omega_0)E_{gi} + \frac{\omega_0}{4K_tV_i}\sum_{k=1}^{N} W_{k,gi}\hat{\Phi}_{k,gi,gj}(g_is_k) + \frac{\omega_0}{4K_tV_i}\sum_{l=1}^{M} W_{gl,gi}\hat{\Phi}_{gl,gi,gj}(g_ig_l) \qquad j = 1, M \tag{23}$$

$\hat{\Phi}_{k,gi,j}$, $\hat{\Phi}_{gl,gi,j}$, and $\hat{\Phi}_{gl,gi,gj}$ are averaged phase functions given by

$$\hat{\Phi}_{k,gi,j} = \frac{K_tV_i}{(g_is_k)(g_is_j)}\int_{A_j}\int_{V_i}\int_{A_k}\Phi(\cos\theta_{jik})e^{-K_t(r_{ji}+r_{ki})} \times \frac{(\mathbf{r}_{ji}\cdot\mathbf{n}_j)(\mathbf{r}_{ki}\cdot\mathbf{n}_k)}{\pi^2 r_{ji}^3 r_{ki}^3}K_t\,dA_k\,dV_i\,dA_j \tag{24}$$

$$\hat{\Phi}_{gl,gi,j} = \frac{K_tV_i}{(g_ig_l)(g_is_j)}\int_{V_l}\int_{V_i}\int_{A_j}\Phi(\cos\theta_{jil})e^{-K_t(r_{ji}+r_{li})} \times \frac{(\mathbf{r}_{ji}\cdot\mathbf{n}_j)}{\pi^2 r_{ji}^2 r_{li}^3}K_t^2\,dV_l\,dV_i\,dA_j \tag{25}$$

and

$$\hat{\Phi}_{gl,gi,gj} = \frac{K_tV_i}{(g_ig_l)(g_ig_j)}\int_{V_l}\int_{V_i}\int_{V_j}\Phi(\cos\theta_{jil})e^{-K_t(r_{ji}+r_{li})} \times \frac{1}{\pi^2 r_{ji}^2 r_{li}^2}K_t^3\,dV_l\,dV_i\,dV_j \tag{26}$$

$\Phi(\cos\theta_{jik})$ is the phase function V_i at $\mathbf{r}_i$ for radiation incident in direction (θ_{ji}, ϕ_{ji}) and being scattered into the (θ_{ik}, ϕ_{ik}) direction. The detailed derivation of Eqs. (20) and (25) are presented in the Appendix. Development of Eqs. (19), (21), (24), and (26) is similar.

Analogous to Eq. (12), Eqs. (13), (14), (15), (16), (17), (18), (22), and (23) can be rewritten as a generalized matrix equation for the generalized radiosity vector $\tilde{\mathbf{W}}$ (composed of the vectors $\mathbf{W}_1, \mathbf{W}_2, \ldots, \mathbf{W}_N, \mathbf{W}_{g1}, \mathbf{W}_{g2}, \ldots, \mathbf{W}_{gM}$):

$$\tilde{\mathbf{W}} = \tilde{X}\tilde{\mathbf{J}} + \tilde{Y}\tilde{\mathbf{W}} \tag{27}$$

where $\tilde{X}$ is a diagonal NM by NM generalized matrix with elements that are NM by NM submatrices. The submatrix elements are functions of ϵ_i, ω_0, A_i, and V_i. $\tilde{Y}$ is a full NM by NM generalized matrix composed of NM by NM submatrices. The submatrix elements of $\tilde{Y}$ are composed of the GZM reflection factors or scattering factors and the CZM exchange factors. $\tilde{\mathbf{J}}$ is a generalized source vector composed of NM subvectors whose components are the specified emissive powers or heat fluxes.

Numerical and Analytical Properties of the Average Scattering Phase Function and Average Reflectivity

It is well known that the CZM exchange factors satisfy reciprocity and closure relations:

$$g_i g_j = g_j g_i \tag{28a}$$

$$g_i s_j = s_j g_i \tag{28b}$$

$$s_i s_j = s_j s_i \tag{28c}$$

$$A_i = \sum_{j=1}^{N} s_i s_j + \sum_{j=1}^{M} s_i g_j \tag{29a}$$

$$4K_t V_i = \sum_{j=1}^{N} g_i s_j + \sum_{j=1}^{M} g_i g_j \tag{29b}$$

In a similar manner, the reflecting and scattering exchange factors also satisfy reciprocity and closure relations:

$$\hat{\rho}_{j,i,k} = \hat{\rho}_{k,i,j} \tag{30a}$$

$$\hat{\rho}_{gj,i,k} = \hat{\rho}_{k,i,gj} \tag{30b}$$

$$\hat{\rho}_{gj,i,gk} = \hat{\rho}_{gk,i,gj} \tag{30c}$$

$$\hat{\Phi}_{j,gi,k} = \hat{\Phi}_{k,gi,j} \tag{31a}$$

$$\hat{\Phi}_{gj,gi,k} = \hat{\Phi}_{k,gi,gj} \tag{31b}$$

$$\hat{\Phi}_{gj,gi,gk} = \hat{\Phi}_{gk,gi,gj} \tag{31c}$$

and for a volume element V_i,

$$4K_tV_i = \sum_{j=1}^{N}(g_is_j)\hat{\Phi}_{k,gi,j} + \sum_{l=1}^{M}(g_ig_l)\hat{\Phi}_{k,gi,gl}$$

$$= \sum_{j=1}^{N}(g_is_j)\hat{\Phi}_{gk,gi,j} + \sum_{l=1}^{M}(g_ig_l)\hat{\Phi}_{gk,gi,gl} \tag{32}$$

for all surface elements A_k and volume elements V_k.

While the numerical evaluation of the reflecting and scattering factors appears to be quite complicated, the computation can be significantly simplified by utilizing some commonly observed properties of surface reflectivity and phase function. For example, the bidirectional reflectivity of many reflecting surfaces can be expressed as a product function:

$$\rho''(\mathbf{r}_i, \theta_{ji}, \phi_{ji}, \theta_{ki}, \phi_{ki}) = \rho'(\mathbf{r}_i, \theta_{ji}, \phi_{ji})\rho'(\mathbf{r}_i, \theta_{ki}, \phi_{ki}) \tag{33}$$

Equation (19) becomes

$$\hat{\rho}_{k,i,j} = \frac{A_i}{(s_is_k)(s_is_j)}\int_{A_i}\hat{\rho}_{j,di}\,\hat{\rho}_{di,k}\,\frac{(ds_is_j)(ds_is_k)}{dA_i} \tag{34}$$

where

$$\hat{\rho}_{j,di} = \hat{\rho}_{di,j} = \frac{dA_i}{ds_is_j}\int_{A_j}\rho'(\mathbf{r}_i, \theta_{ji}, \phi_{ji})e^{-K_t(r_{ji})}\frac{(\mathbf{r}_{ji}\cdot\mathbf{n}_i)(\mathbf{r}_{ji}\cdot\mathbf{n}_j)}{\pi r_{ji}^4}\,dA_j \tag{35}$$

Equation (19) initially requires a triple area integral, a sixfold integration. By using Eq. (35), the integration in Eq. (19) is reduced to an area integral of the product of area integrals (equivalent to three twofold integrations). This is a substantial reduction in computational complexity. Similar simplification can be achieved for Eqs. (20) and (21).

The phase function of many scattering media can be expressed as a power series in $\cos\theta_{jik}$. The power series can be expressed in terms of the vectors $\mathbf{r}_{jk} = (x_{jk}, y_{jk}, z_{jk})$ and $\mathbf{r}_{ij} = (x_{ij}, y_{ij}, z_{ij})$:

$$\Phi(\cos\theta_{jik}) = \sum_n C_n\cos^n(\theta_{jik}) = \sum_n C_n\left(\frac{\mathbf{r}_{ji}\cdot\mathbf{r}_{ik}}{r_{ji}r_{ik}}\right)^n$$

$$= \sum_n C_n\sum_{p+q+l=n}\left(\frac{x_{ji}^p y_{ji}^q z_{ji}^l}{r_{ji}^n}\right)\left(\frac{x_{ik}^p y_{ik}^q z_{ik}^l}{r_{ik}^n}\right) \tag{36}$$

Equation (24), the scattering exchange factor between A_j and A_k via V_i, becomes

$$\hat{\Phi}_{k,gi,j} = \sum_n C_n \hat{\Phi}^{[n]}_{k,gi,j} \tag{37}$$

with

$$\hat{\Phi}^{[n]}_{k,gi,j} = \frac{V_i}{(g_i s_k)(g_i s_j)} \int_{V_i} \hat{\Phi}^{[n]}_{j,dgi} \hat{\Phi}^{[n]}_{dgi,k} \frac{(s_j\, dg_i)(s_k\, dg_i)}{dV_i} \tag{38}$$

where

$$\hat{\Phi}^{[n]}_{j,dgi} = \hat{\Phi}^{[n]}_{dgi,j} = \sum_{p+q+l=n} \frac{dV_i}{(s_j\, dg_i)} \int_{A_j} \frac{K_t e^{-K_t r_{ji}} (\mathbf{r}_{ji} \cdot \mathbf{n}_j) x_{ji}^p y_{ji}^q z_{ji}^l}{\pi r_{ji}^{3+n}} dA_j \tag{39}$$

As in the case of the reflecting factor, the evaluation of $\hat{\Phi}_{k,gi,j}$ is reduced from a sevenfold integral to the sum of fivefold integrals. Equations (25) and (26) can be similarly reduced.

In short, the numerical computation of the average reflectivity and average scattering phase function has the same level of complexity as the evaluation of conventional exchange factors. In comparison to CZM, the only mathematical complexity introduced by GZM is the introduction of the concept of radiosity vector.

IMPLEMENTATION

To demonstrate the effectiveness of the GZM, cubical enclosures of with a range of optical thicknesses were analyzed. The specific geometry and coordinate system are shown in Figure 1. The bottom surface (A_6) is black and hot with a unit emissive power, while the remaining five surfaces are black and cold with zero emissive power. The medium is at radiative equilibrium and has a linear anisotropic scattering phase function given by

$$\Phi(\theta) = 1 + \beta \cos\theta \tag{40}$$

The number of zones used in the analysis was progressively increased in order to prove convergence. The first analysis was with one volume zone ($N_z = 1$) for the entire medium and six surface zones, one for each wall. The next analysis used eight volume zones ($N_z = 2$; $2 \times 2 \times 2$ grid) and 24 surface zones. The final analysis used 64 volume zones ($N_z = 4$; $4 \times 4 \times 4$ grid) and 96 surface zones. It should be noted that the complexity of the analysis grows quite rapidly. It will be shown later that the one-volume-zone analysis could be done in closed form. The eight-volume-zone analysis had 16 unknowns; the 64-zone analysis had 192 unknowns.

The presentation in this section will be in three parts. In the first section the one-zone analysis will be presented in detail. This will illustrate some unique features of the GZM. In the second section, grid size convergence will be shown. Lastly, numerical results will be presented.

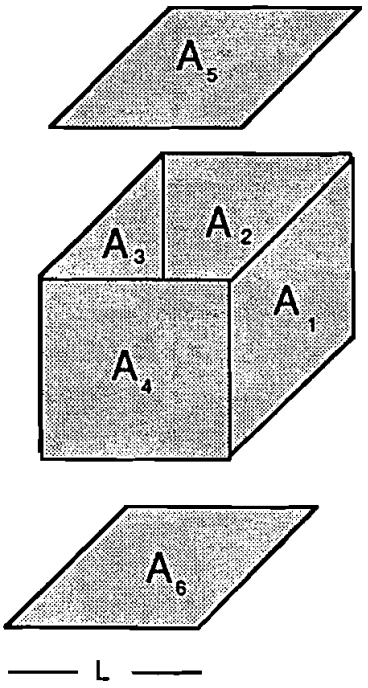

Figure 1. Geometry and area identification for the cubical enclosure (the top and bottom surfaces are removed for improved clarity in area identification).

One-Zone Analysis

In the one-zone analysis the entire medium is treated as a single volume zone and each wall as a single surface zone. To simplify the notation, the subscript g is used for the single volume zone. Since all surfaces are black, the radiosity on each surface is known (1 for A_6 and 0 for the remaining surfaces). From Eq. (15), the heat transfer at the six surfaces is given below.

$$Q_i = -(s_6 s_i) - (g s_i) W_{g,i} \qquad i = 1, \ldots, 5 \tag{41a}$$

and

$$Q_6 = 1 - (g s_6) W_{g,6} \tag{41b}$$

The radiosity components for the gas zone can be deduced from Eq. (22) to yield

$$W_{g,j} = (1 - \omega_0) E_g + \frac{\omega_0}{4 K_t V_g} \left[\hat{\Phi}_{6,g,j} (g s_6) + \hat{\Phi}_{g,g,j} (gg) W_{g,g} \right] \qquad j = 1, \ldots, 6 \tag{42a}$$

and

$$W_{g,g} = (1 - \omega_0)E_g + \frac{\omega_0}{4K_tV_g}\left[\hat{\Phi}_{6,g,g}(gs_6) + \hat{\Phi}_{g,g,g}(gg)W_{g,g}\right] \qquad (42b)$$

E_g, the average emissive power of the medium, can be deduced by combining Eqs. (16) and (42b) to yield

$$E_g = \frac{(s_6g)\left[1 - (\omega_0/4K_tV_g)(gg)\left(\hat{\Phi}_{g,g,g} - \hat{\Phi}_{6,g,g}\right)\right]}{4K_tV_g - (gg) + \omega_0(gg)\left(1 - \hat{\Phi}_{g,g,g}\right)} \qquad (43)$$

Equations (42a) and (42b) illustrate that the components of the radiosity vector, $W_{g,i}$, are not identical in general. While this is expected for anisotropically scattering media, it is true even for an isotropically scattering medium. This is a direct contradiction of CZM intuition, which indicates that all components of the radiosity vector should be equal. This contradiction can be explained both physically and mathematically.

Physically, the imbalance reflects the anisotropic nature of the boundary conditions (unit emissive power at the bottom wall and zero emissive power elsewhere). For a single volume zone, it is clear that the radiosity components to the top wall and side walls cannot be equal.

Mathematically, the equations for radiosity components use the scattering factors to show the effects of geometry and scattering phase function. Note that even for an isotropic scattering medium, the scattering factor is unity only for a differential volume element dV_{gi}; that is,

$$\hat{\Phi}_{j,dgi,k} = \hat{\Phi}_{gj,dgi,k} = \hat{\Phi}_{gj,dgi,gk} = 1.0 \qquad (44)$$

The scattering factors for a finite volume element, V_{gi}, on the other hand, are unequal and given by

$$\hat{\Phi}_{k,gi,j} = \frac{V_i}{(g_is_k)(g_is_j)}\int_{V_i}\frac{(s_j\,dg_i)(s_k\,dg_i)}{dV_i} \qquad (45)$$

The difference in exchange factors leads to the difference in the radiosity components. The difference in isotropic results disappears as the number of zones taken in the CZM and GZM analyses increases. But for the same number of zone, the GZM is clearly an improvement over the CZM, even for isotropic analysis.

It is interesting to note that utilizing the appropriate summation rule for exchange factors and scattering factors, Eq. (43), in the limit of a cubic enclosure, is reduced to

$$E_g = \frac{1}{6} \qquad (46)$$

This is the expected result from superposition and the same result as a one-zone CZM analysis. This reaffirms that the difference between the CZM and GZM is in

the treatment of scattering. From examining Eqs. (42*a*) and (42*b*), it is clear that the CZM and GZM are identical if there is no scattering ($\omega_0 = 0$).

Convergence

To illustrate their effect on radiative transfer, the optical thickness, scattering albedo, and scattering phase function were varied. Runs were made for optical thickness $L = 0.1, 0.5, 1.0, 2.0, 3.0$; scattering albedo $\omega_0 = 0, 0.2, 0.4, 0.6, 0.8, 1$; and linear scattering coefficient $\beta = -1, 0, 1$. In order to claim benchmark status for these results, grid size convergence must be shown.

The bottom, side, and top wall fluxes $q_b = Q_6/L^2$, $q_s = -Q_1/L^2$, $q_t = -Q_5/L^2$ for various grids are shown in Table 1. Results for $\omega_0 = 1$ were chosen because they are "pure" GZM results; the results are entirely dominated by scattering. The table shows that the fluxes have converged to within 5% for the bottom and side walls and within 0.015 for the top wall (the top wall convergence is slow because of the small dimensionless heat flux). for $L = 0.1$, an optically thin case, only eight volume zones ($n_z = 2$) are necessary for convergence. For all other optical thicknesses, 64 volume zones ($n_z = 4$) are required.

In Figure 2, the convergence behavior of a pure isotropic scattering ($\omega = 1$) GZM solutions ($N_z = 1, 2, 4$) is shown and compared to the corresponding CZM results. These results represent numerical proof of the earlier statement that, given the same number of zones, GZM solutions are more accurate than CZM. This increased accuracy compensates for the increased effort required by the GZM.

Results

To illustrate the effect of optical thickness, geometry, and scattering phase function on the heat transfer, the average heat transfer from the bottom, top, and side walls are tabulated and presented in Table 2 and Figures 3, 4, and 5. In Table 2, the no-scattering results are presented for different optical thickness, L. In Figures 3, 4, and 5, the percentage change in the three average fluxes, B, T, and S, are defined by

$$B = \left[\frac{q_b \text{ (with scattering)}}{q_b \text{ (no scattering)}} - 1\right]100 \tag{47}$$

$$S = \left[\frac{q_s \text{ (with scattering)}}{q_s \text{ (no scattering)}} - 1\right]100 \tag{48}$$

$$T = \left[\frac{q_t \text{ (with scattering)}}{q_t \text{ (no scattering)}} - 1\right]100 \tag{49}$$

In general, optical thickness, scattering albedo, and the forward/backward scattering parameter, β, have significant effect on heat transfer. The effect on the

Table 1. Convergence Behavior of the GZM Solutions for Different Optical Thicknesses and Scattering Parameters

			(*a*) $L = 0.1$; $\omega_0 = 1.0$			
	q_b		q_s		q_t	
β	$n_z = 1$	$n_z = 2$	$n_z = 1$	$n_z = 2$	$n_z = 1$	$n_z = 2$
−1	0.9808	1.0000	0.1990	0.2000	0.1866	0.2000
0	0.9890	1.0000	0.2000	0.2000	0.1890	0.2000
1	1.0000	1.0000	0.2017	0.2000	0.1909	0.2000
			(*b*) $L = 0.5$; $\omega_0 = 1.0$			
	q_b		q_s		q_t	
β	$n_z = 2$	$n_z = 4$	$n_z = 2$	$n_z = 4$	$n_z = 2$	$n_z = 4$
−1	0.9016	0.8995	0.1964	0.1958	0.1299	0.1334
0	0.9300	0.9280	0.2004	0.1999	0.1422	0.1454
1	0.9590	0.9580	0.2045	0.2040	0.1552	0.1585
			(*c*) $L = 1.0$; $\omega_0 = 1.0$			
	q_b		q_s		q_t	
β	$n_z = 2$	$n_z = 4$	$n_z = 2$	$n_z = 4$	$n_z = 2$	$n_z = 4$
−1	0.8299	0.8248	0.1872	0.1873	0.0897	0.0917
0	0.8730	0.8691	0.1943	0.1945	0.1046	0.1065
1	0.9171	0.9163	0.2014	0.2020	0.1208	0.1239
			(*d*) $L = 2.0$; $\omega_0 = 1.0$			
	q_b		q_s		q_t	
β	$n_z = 2$	$n_z = 4$	$n_z = 2$	$n_z = 4$	$n_z = 2$	$n_z = 4$
−1	0.7390	0.7227	0.1722	0.1705	0.0537	0.0516
0	0.7938	0.7809	0.1829	0.1816	0.0666	0.0648
1	0.8497	0.8432	0.1935	0.1931	0.0810	0.0812
			(*e*) $L = 3.0$; $\omega_0 = 1.0$			
	q_b		q_s		q_t	
β	$n_z = 2$	$n_z = 4$	$n_z = 2$	$n_z = 4$	$n_z = 2$	$n_z = 4$
−1	0.6809	0.6553	0.1597	0.1573	0.0389	0.0341
0	0.7442	0.7174	0.1721	0.1702	0.0487	0.0442
1	0.7978	0.7834	0.1844	0.1836	0.0596	0.0571

bottom wall and side wall heat transfer is similar because, except for cases with small optical thickness, most of the heat loss from the bottom wall is transferred to the side walls. Specifically, for both the isotropic scattering ($\beta = 0$) and backward scattering ($\beta = -1$) cases, heat transfer decreases with increasing albedo and increasing optical thickness. The percentage change can be as high as 13% for the case with large optical thickness and large scattering albedo (e.g., heat transfer from the bottom wall with $L = 3.0$, $\omega_0 = 1.0$, and $\beta = -1$). For the case with

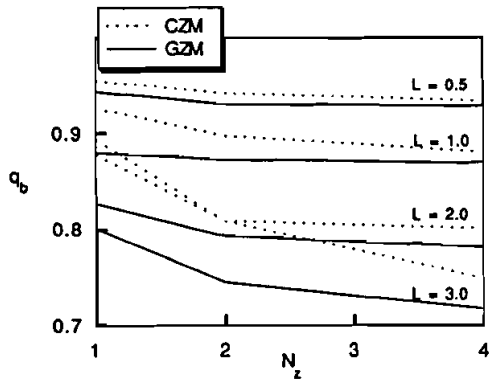

Figure 2. Convergence behavior for GZM and CZM for the isotropic scattering results.

forward scattering ($\beta = 1$), on the other hand, heat transfer increases with increasing albedo. The magnitude of change is smaller (maximum change is 5% for $L = 2.0$, $\omega_0 = 1.0$) and does not increase monotonically as optical thickness increases. The asymmetric effect of β on the heat transfer at the bottom wall and side walls can be attributed to the combined effect of geometry and multiple scattering. In an isotropic scattering and strongly backward scattering medium, an increase in the scattering albedo redirects much of the emitted energy back to the bottom wall, so the net heat transfer decreases. While the energy emitted by the bottom wall is scattered forward in a forward scattering medium, much of the energy is absorbed by the medium and reemitted back to the bottom wall. this effect is particularly strong in a medium with large optical thickness and small scattering albedo. This explains the relatively small effect of the scattering albedo on heat transfer at the bottom and side walls in a forward scattering medium.

The forward/backward scattering parameter has a more symmetric effect on the heat transfer to the top wall, as shown in Figure 5. Physically, a large fraction of the heat transfer to the top wall is due to the reemission of the medium. The directional effect of the scattering phase function is thus expected to have less influence on the heat transfer. As shown by the no-scattering results in Table 2, the magnitude of heat transfer to the top wall is relatively small, particularly in cases with moderate and large optical thickness. This leads to the relatively large

Table 2. Heat Flux at the Top, Bottom, and Side Walls for a Nonscattering Medium Predicted by GZM

L	q_b	q_s	q_t
0.1	1.000	0.200	0.200
0.5	0.938	0.201	0.148
1.0	0.881	0.195	0.107
2.0	0.802	0.185	0.067
3.0	0.749	0.177	0.047

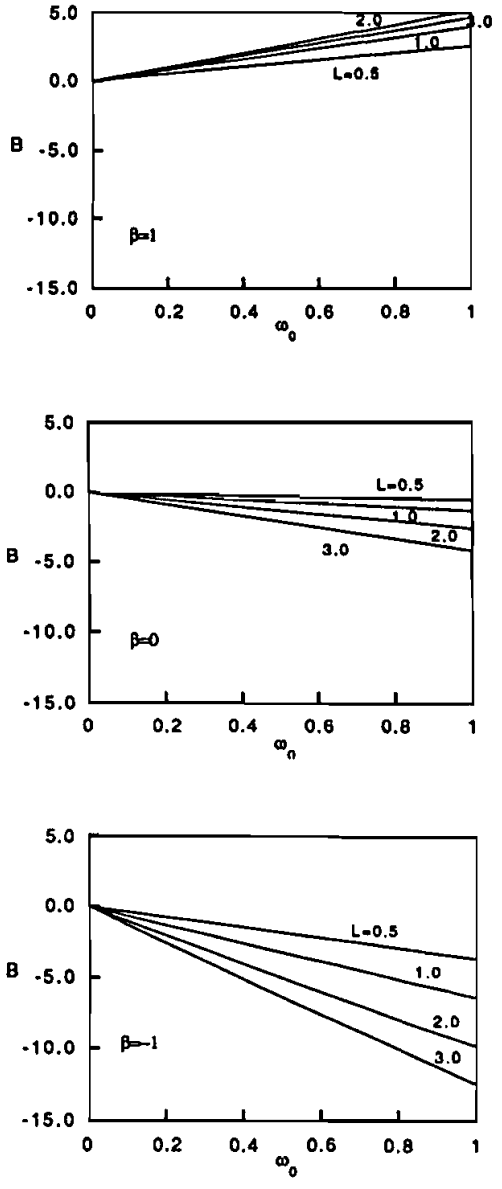

Figure 3. Effect of optical thickness and scattering on heat transfer from the bottom wall.

percentage change in the heat transfer to the top wall as the scattering albedo increases.

CONCLUSION

The basic formulation for GZM has been presented and implemented. Cubical enclosures in radiative equlibrium with varying optical thickness and

scattering properties were analyzed. It was demonstrated that the GZM can be an effective solution technique for two reasons. First, it is unique in its ability to model anisotrpic scattering. Second, by improving the modeling of scattering, a smaller number of zones is required to reach a converged solution.

The results presented showed that the effect of anisotropic scattering on three-dimensional radiative heat transfer is clearly important. Both geometry and scattering parameters have significant influence on the overall heat transfer. These effects cannot be simulated with a one-dimensional study.

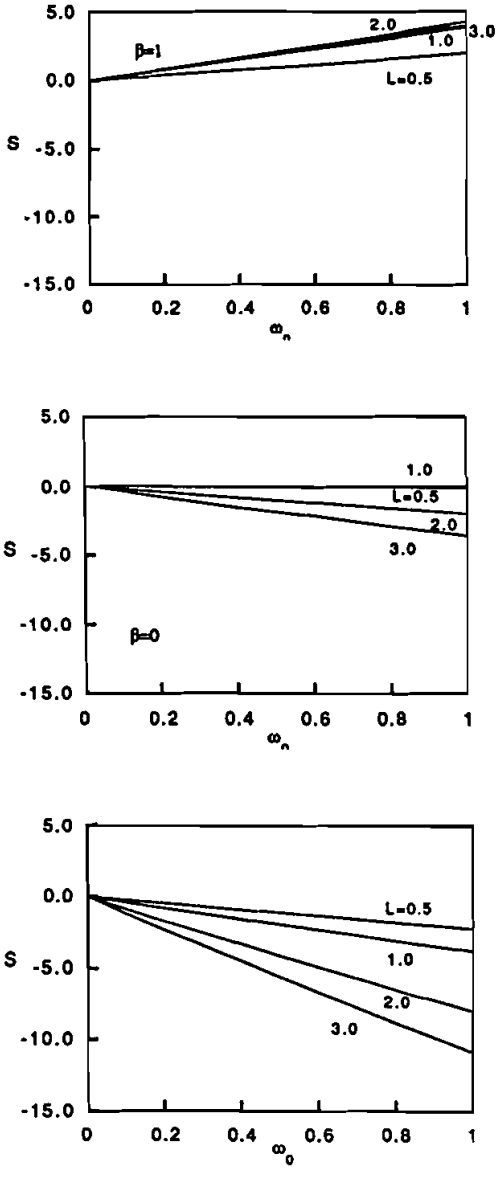

Figure 4. Effect of optical thickness and scattering on heat transfer to the side wall.

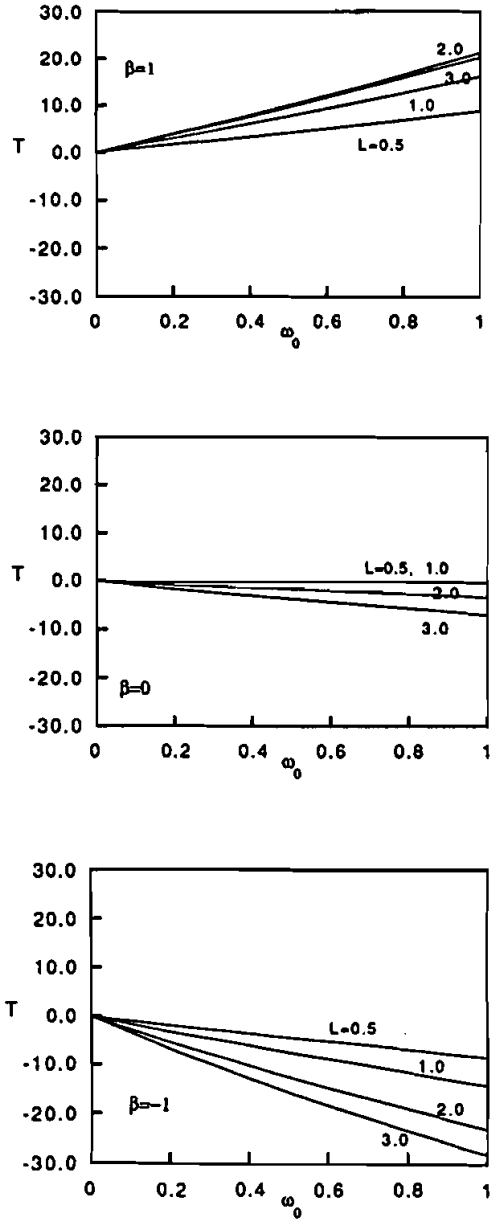

Figure 5. Effect of optical thickness and scattering on heat transfer to the top wall.

While the applicability of the GZM has been demonstrated, its implementation can be improved. The number of scattering factors to calculate can become truly daunting. Parallel computing should be considered to overcome this. Also, other phase functions should be examined. A combined Monte Carlo GZM hybrid can be used for the more difficult phase functions.

APPENDIX

For the development of Eq. (20), consider a volume zone V_j and two area zones A_i, A_k, as shown in Figure A1. The net outgoing radiation from a differential volume dV_j, reflected by a differential area dA_i and intercepted by a differential area dA_k, can be written as

$$d^3Q_{gj,i,k} = i'_{gj,i}(\mathbf{r}_j)\rho''(\mathbf{r}_i, \theta_{ji}, \phi_{ji}, \theta_{ki}, \phi_{ki})e^{-K_t(r_{ji}+r_{ki})} \times \frac{(\mathbf{r}_{ji}\cdot\mathbf{n}_i)(\mathbf{r}_{ki}\cdot\mathbf{n}_i)(\mathbf{r}_{ki}\cdot\mathbf{n}_k)}{r_{ji}^3 r_{ki}^4} K_t\, dV_j\, dA_i\, dA_k \tag{A1}$$

In terms of the net outgoing radiosity $dW_{gj,i}$, the intensity $i'_{gj,i}$ can be written as

$$i'_{gj,i} = \frac{dW_{gj,i}}{\pi} \tag{A2}$$

Utilizing Eqs. (1), (2), and (3), Eq. (A1) become

$$d^3Q_{gj,i,k} = \frac{\pi\, dW_{gj,i}}{dA_i}\rho''(\mathbf{r}_i, \theta_{ji}, \phi_{ji}, \theta_{ki}, \phi_{ki})(ds_i\, dg_j)(ds_i\, ds_k) \tag{A3}$$

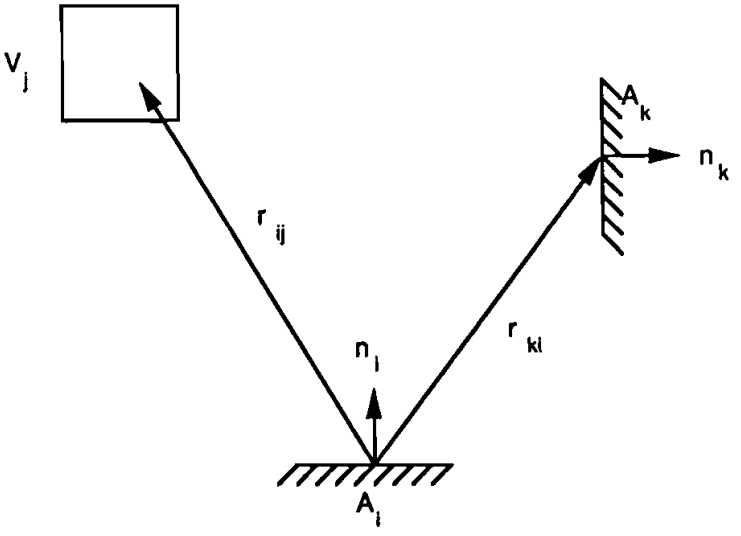

Figure A1. Geometry and notation used in the development of Eq. (20).

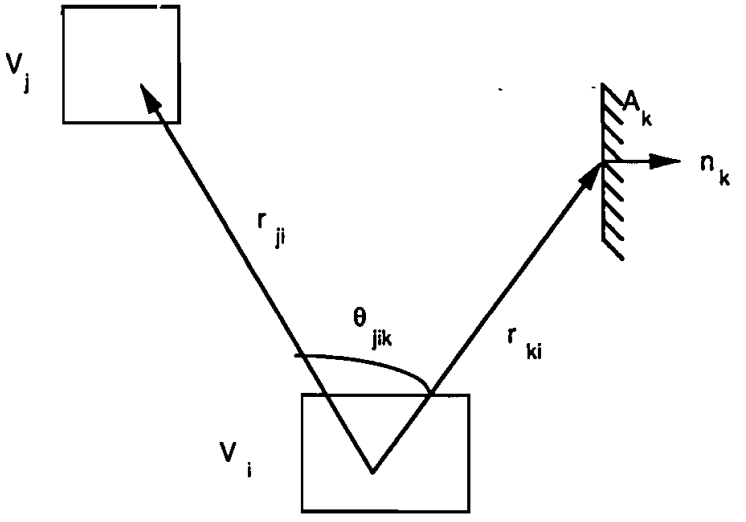

Figure A2. Geometry and notation used in the development of Eq. (25).

In GZM, the radiosity from V_{gj} directed toward A_i is assumed to be constant. Integrating over V_{gj}, A_i, and A_k, Eq. (A3) becomes

$$Q_{gj,i,k} = \frac{\pi}{A_i} W_{gj,i}(s_i g_j)(s_i s_k)\hat{\rho}_{gj,i,k} \tag{A4}$$

with $\hat{\rho}_{gj,i,k}$ given by Eq. (20).

Equation (25) can be derived in a similar manner. Utilizing the geometry and notations as shown in Figure A2, the net outgoing radiation from a differential volume dV_j, reflected by a differential volume dV_i and intercepted by a differential area dA_k can be written as

$$d^3Q_{gj,gi,k} = i'_{gj,gi}(\mathbf{r}_j)\omega_0 \frac{\Phi(\cos\theta_{jik})}{4\pi} e^{-K_t(r_{ji}+r_{ki})} \frac{(\mathbf{r}_{ki}\cdot\mathbf{n}_k)}{r_{ji}^2 r_{ki}^3} K_t^2\, dV_j\, dV_i\, dA_k \tag{A5}$$

In terms of the radiosity $dW_{gj,gi}$ and the various differential exchange factors, Eq. (A5) becomes

$$d^3Q_{gj,gi,k} = \frac{\omega_0\, dW_{gj,gi}}{4K_t\, dV_i}\Phi(\cos\theta_{jik})(dg_i\, dg_j)(dg_i\, ds_k) \tag{A6}$$

Integrating over the finite volumes and area, Eq. (A6) becomes

$$Q_{gj,gi,k} = \frac{\omega_0}{4K_t V_i} W_{gj,gi}(g_i g_j)(g_i s_k)\hat{\Phi}_{gj,gi,k} \tag{A7}$$

with $\hat{\Phi}_{gj,gi,k}$ given by Eq. (25).

REFERENCES

1. R. Viskanta, Radiative Heat Transfer Interaction with Conduction and Convection, and Approximate Methods in Radiation, *Proc. Seventh Int. Heat Transfer Conf.*, vol. 1, pp. 103–122, 1982.
2. A. F. Sarofim, Radiative Heat Transfer in Combustion: Friend or Foe, *Twenty First Symp. (Int.) on Combustion*, The Combustion Institute, Pittsburgh, pp. 1–23, 1986.
3. R. Viskanta and M. P. Menguc, Radiation Heat Transfer in Combustion Systems, *Prog. Energy Combustion Sci.*, vol. 13, pp. 97–160, 1987.
4. E. Ozil and R. C. Birkebak, Effect of Environmental Radiation in the Insulative Properties of a Fibrous Material, *Proc. Seventh Symp. on Thermophysical Properties*, ASME, New York, pp. 319–327, 1977.
5. C. G. Bankvall, Heat Transfer in Fibrous Materials, *J. Testing Eval.*, vol. 1, pp. 235–243, 1973.
6. T. W. Tong, Q. S. Yang, and C. L. Tien, Radiative Heat Transfer in Fibrous Insulations, Part II: Experimental Study, *J. Heat Transfer*, vol. 105, pp. 76–81, February 1983.
7. A. Schuster, Radiation through a Foggy Atmosphere, *Astrophys. J.*, vol. 21, pp. 1–22, 1905.
8. K. Schwarzschild, Equilibrium of the Sun's Atmosphere, *Nachr. Math. Phys. Klasse*, vol. I, pp. 41–53, 1906.
9. C. M. Chu and S. W. Churchill, Numerical Solutions of Problems in Multiple Scattering of Electromagnetic Radiation, *J. Phys. Chem.*, vol. 59, pp. 855–863, 1960.
10. R. G. Siddall and N. Selcuk, Evaluation of a New Six-Flux Model for Radiative Heat Transfer in Rectangular Enclosure, *Trans. Inst. Chem. Eng.*, vol. 57, pp. 163–169, 1979.
11. M. N. Abramzon and F. N. Lisin, *High Temperature*, vol. 22, p. 95, 1984.
12. A. G. DeMarco and F. C. Lockwood, A New Flux Model for the Calculation of Radiation in Furnaces, *La Rivista dei Combustibli*, vol. 29, pp. 184–196, 1975.
13. F. C. Lockwood and N. G. Shah, Evaluation of an Efficient Radiation Flux Model for Furnace Prediction Procedures, *Proc. Sixth Int. Heat Transfer Conf.*, vol. 2, pp. 33–40, 1978.
14. B. Davison, *Neutron Transport Theory*, Clarendon Press, Oxford, 1958.
15. M. P. Menguc and R. Viskanta, Radiative Transfer in Three-Dimensional Rectangular Enclosures, *J. Quant. Spectrosc. Radiative Transfer*, vol. 33, pp. 533–549, 1985.
16. K. D. Lathrop, THREETRAN—A Program to Solve the Multigroup Discrete Ordinates Transport EQuations in (x, y, z) Geometry, Report LA-6333-MS, Los Alamos Scientific Laboratory, 1976.
17. W. A. Fiveland, Discrete-Ordinates Solutions of the Radiative Transport Equation for Rectangular Enclosure, *J. Heat Transfer*, vol. 106, pp. 699–706, 1984.
18. H. C. Hottel and A. F. Sarofim, *Radiative Transfer*, McGRaw-Hill, New York, 1967.
19. J. R. Howell and M. Perlmutter, Monte Carlo Solution of Radiant Heat Transfer in a Nongrey Nonisothermal Gas with Temperature Dependent Properties, *AIChE J.*, vol. 10, pp. 562–567, 1964.
20. H. Taniguchi, The Radiative Heat Transfer of Gas in a Three-Dimensional System Calculated by Monte Carlo Method, *Bull. JSME*, vol. 12, pp.67–78, 1969.
21. M. P. Menguc and R. Viskanta, *J. Heat Transfer*, vol. 108, p. 271, 1986.
22. T. W. Tong and R. D. Skocypec, Summary on Comparison of Radiative Heat Transfer Solutions for a Specified Problem, in T. W. Tong and R. D. Skocypec (eds.), *Developments in Radiative Heat Transfer*, ASME HTD Vol-13, pp. 253–258, 1992.
23. W. W. Yuen, A. Ma, and E. E. Takara, Evaluation of Radiative Heat Transfer Using the Generalized Zonal Method and the Absorption Mean Beam Length Concept, in T. W. Tong and R. D. Skocypec (eds.), *Developments in Radiative Heat Transfer*, ASME HTD Vol-13, pp. 265–274, 1992.

24. M. H. N. Naraghi, Solution to the Benchmark Problem Using Discrete Exchange Factor Method, in T. W. Tong and R. D. Skocypec (eds.), *Developments in Radiative Heat Transfer*, ASME HTD Vol-13, pp. 275–284, 1992.
25. P. Hsu, Z. Tan, and J. R. Howell, Application of the YIX Method to Radiative Heat Transfer within a Mixture of Highly Anisotropic Scattering Particles and Non-Gray Gas, in T. W. Tong and R. D. Skocypec (eds.), *Developments in Radiative Heat Transfer*, ASME HTD Vol-13, pp. 285–300, 1992.
26. J. T. Farmer and J. R. Howell, Monte Carlo Solution of Radiative Heat Transfer in a Three Dimensional Enclosure with an Anisotropically Scattering, Spectrally Dependent, Inhomogeneous Medium," in T. W. Tong and R. D. Skocypec (eds.), *Developments in Radiative Heat Transfer*, ASME HTD Vol-13, pp. 301–310, 1992.
27. K. C. Tang and M. Q. Brewster, K-Distribution Analysis of Gas Radiation with Non-Gray, Emitting, Absorbing, and Anisotropic Scattering Particles, in T. W. Tong and R. D. Skocypec (eds.), *Developments in Radiative Heat Transfer*, ASME HTD Vol-13, pp. 311–320, 1992.
28. D. K. Edwards, Hybrid Monte-Carlo Matrix-Inversion Formulation of Radiation Heat Transfer with Volume Scattering, *Heat Transfer in Fire and Combustion System*, ASME HTD-Vol. 45, pp. 273–278, 1985.
29. W. W. Yuen, Development of a Network Analogy and Evaluation of Mean Beam Lengths for Multi-Dimensional Absorbing/Isotropically Scattering Media, *J. Heat Transfer*, vol. 112, pp. 408–413, 1990.